# Miniaturizing optical antennas using hyperbolic metamaterial wires

Rafik Smaali, Fatima Omeis, Antoine Moreau, and Emmanuel Centeno*
*Université Clermont Auvergne, CNRS, SIGMA Clermont, Institut Pascal, F-63000 Clermont-Ferrand, France*

Thierry Taliercio
*Université Montpellier, IES, UMR 5214 and CNRS, IES, UMR 5214, F-34000 Montpellier, France*
(Received 5 December 2016; revised manuscript received 14 March 2017; published 7 April 2017)

We propose the concept of hyperbolic wires that overcome the actual limitation of metal-insulator-metal (MIM) patch antennas in terms of electromagnetic confinement and efficiency. The use of hyperbolic metamaterials allows one to realize miniaturized resonators sustaining bulk plasmon polaritons squeezed to only one-hundredth of the wavelength. Beyond this tenfold size reduction compared to MIM antennas, we propose a model allowing one to scale the resonant frequencies of hyperbolic wires over a broad spectral range by controlling the filling ratio in metals and dielectrics.

DOI: 10.1103/PhysRevB.95.155306

## I. INTRODUCTION

Optical plasmonic nanoantennas offer fascinating ways to manipulate electromagnetic radiations at a deeply subwavelength scale [1]. Among the different geometries that have been considered, optical patch antennas, also known as metal-insulator-metal (MIM) structures or gap-plasmon resonators, have in particular proven to be an efficient approach for many optical applications ranging from spectroscopy, light emission, or biosensing to photovoltaics [2–7]. The geometry of a MIM resonator is extremely similar to that of microwave patch antennas, except for the ratio between the operation wavelength $\lambda_r$ and the size of the patch. In the microwave range the typical width of the patch is $\lambda_r/2$, while optical patch antennas are much smaller than the wavelength because they operate close enough to the plasma frequency of metals and thus benefit from the plasmonic nature of metals.

A MIM antenna is constituted of a metallic patch (for example, a cube, a cross, or a wire) separated from a metallic substrate by a dielectric spacer [Fig. 1(a)]. This structure sustains a peculiar guided mode called a gap plasmon [8] which propagates in the dielectric spacer, along the metallic planes. This mode presents a very high effective index $n_{\text{eff}}$, and thus a very short effective wavelength. It is reflected by the edges of the patch, so that the structure forms an actual Fabry-Perot cavity, whose fundamental resonant wavelength is typically given by $\lambda_r = 2n_{\text{eff}}w$ where $w$ is the width of the resonator [9]. The ratio between the width of the resonator and its operating wavelength is critical: It is directly linked to the ability of the resonator to concentrate light efficiently and to produce various phenomena [10–12]. It can be quantified by introducing a miniaturization parameter $m_p = \lambda_r/w$. For MIM structures with a dielectric spacer of thickness $g$, $m_p$ is proportional to the effective index of the gap plasmon that can be approximated by $n_{\text{eff}} = \sqrt{\epsilon_d}\sqrt{1 + 2\delta_p/g}$ where $\delta_p = c/\omega_p$ is the penetration depth into the metal and $\epsilon_d$ is the permittivity of the dielectric spacer [13–15]. Increasing the effective index by decreasing the thickness $g$ of the spacer is thus a simple way to miniaturize the plasmonic antenna [Fig. 1(b)]. For example, in Refs. [16,17] a ratio $m_p = 10$ is reached for nanocubes placed above a dielectric spacer presenting a subwavelength thickness of $\lambda/70$ in the visible, which represents only a few nanometers.

Beyond the simple miniaturization of resonators, a high effective index for the gap plasmon is accompanied by a slow light effect which is highly desirable to enhance light-matter interaction [18–20]. Using high effective index modes is thus a strategy for enhancing the nonlinear effects or to reduce the lifetime of an emitter placed under the patches [21–23]. This Purcell effect, giant as it may be, occurs when the gap $g$ is very small and when the cavity is only barely coupled to the outside continuum, making the emitting device much less efficient than what could be expected. For instance, when ultrathin spacers are considered, the incident light is unable to couple with the gap plasmon mode leading to an inefficient absorption [Fig. 1(c)]. To summarize, the resonator becomes intrinsically inefficient beyond a ratio $m_p$ of typically 10–20 [24].

Here we propose to reach both higher miniaturization ratios and higher efficiencies by replacing the dielectric spacer by a hyperbolic metamaterial (HM) layer, as shown Fig. 2. Such a HM spacer actually supports guided modes named bulk plasmon polaritons (BPPs) [25] with an even higher effective index than gap plasmons, allowing one to reach a miniaturization ratio of $m_p = 100$, while staying much thicker, thus ensuring an efficient coupling to the continuum. We call these structures hyperbolic wires (HWs).

As is common with patch antennas, two-dimensional (2D) and three-dimensional (3D) resonators share the same physical principles but do not have exactly the same overall optical response. In a first part, we thus propose a thorough physical analysis of a 2D hyperbolic wire and a model for the resonators that we compare to full simulations. In a second part, we extend our analysis to the full 3D case.

## II. EFFECTIVE PROPERTIES OF HYPERBOLIC WIRES

Hyperbolic metamaterials are a class of artificial anisotropic materials that consist of a periodic metallodielectric structures presenting hyperboloid isofrequency surfaces [26–28], hence their name. When the period is much smaller than the

*emmanuel.centeno@univ-bpclermont.fr

 ©2017 American Physical Society

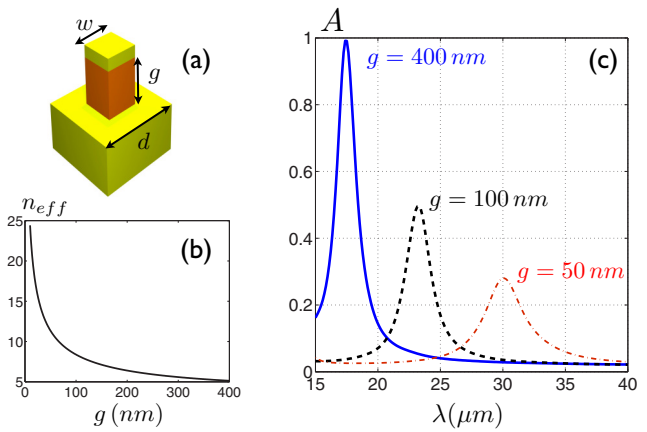


FIG. 1. (a) Schematic of a MIM antenna. (b) Effective index of the gap plasmon as a function of $g$. (c) Absorption spectrum calculated in normal incidence for a MIM antenna composed of InAsSb-GaSb-InAsSb for a period $d = 5\ \mu$m, a width $w = 1\ \mu$m, and for three spacer thicknesses $g = \{50, 100, 400\}$ nm. The thickness of the metallic antenna is 300 nm. The absorption decreases when the spacer thickness decreases.

wavelength, these multilayers behave as a homogeneous medium characterized by an effective permittivity tensor $\bar{\epsilon}$ whose principal elements are $\epsilon_x$, $\epsilon_y$, and $\epsilon_z$. Two kinds of HMs have to be distinguished. Type-I HMs present a negative permittivity in the extraordinary direction ($\epsilon_z < 0$) and positive permittivities in the ordinary directions ($\epsilon_x > 0$ and $\epsilon_y > 0$). Meanwhile, type-II HMs have one dielectriclike component ($\epsilon_z > 0$) and two metalliclike components ($\epsilon_x < 0$ and $\epsilon_y < 0$). Nanowire-, grating-, or multilayer-based structures are the main approaches allowing one to design both types of HMs [29–31]. Stacks of metallic and dielectric films have, in particular, been considered for realizing flat lenses [32,33] and absorbers or polarizers when an additional structuring is employed [34–36]. A rainbow trapping effect has been demonstrated with tapered HMs of type-II supporting slow guided modes propagating in the extraordinary direction where $\epsilon_z > 0$. Their broad spectral response is due to the varying width of those tapered waveguides between a tenth to a quarter

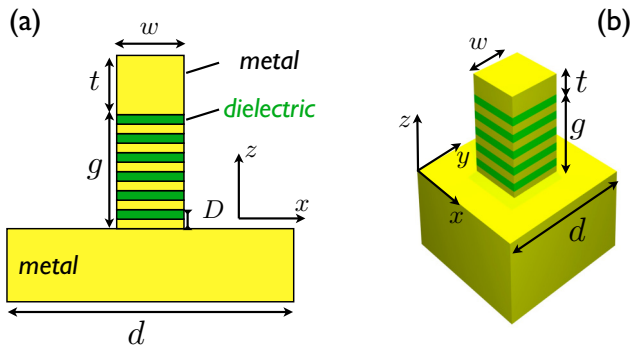


FIG. 2. Schematics of the unit cell for a metallic patch suspended over a hyperbolic wire placed on a metallic substrate. (a) and (b) correspond, respectively, to the 2D and 3D cases.

of the incident wavelength [37]. Here, a metallodielectric multilayer belonging to the type-II category is also considered but the miniaturization effect is obtained for modes guided in the ordinary direction (i.e., perpendicular to the $z$ direction). We demonstrate that similarly to MIM patch antennas, these modes recognized as BPPs resonate in a cavity whose width is determined by their effective index [25,31,38].

We consider a 2D metallic patch of width $w$ and thickness $t$ placed on top of a hyperbolic wire which consists of periodic stack of metal and dielectric layers with respective thicknesses and permittivities $(h_m, \epsilon_m)$ and $(h_d, \epsilon_d)$, as shown Fig. 2(a). Note that the metallic patch and substrate are made with the same metal of permittivity $\epsilon_m$. The dielectric filling factor is defined by $\rho = h_d/D$ where $D$ is the lattice period of the multilayer ($D = h_m + h_d$). This theoretical study actually holds for any medium that can be described by the Drude model, whether it is a metal, strictly speaking, or a highly doped semiconductor. Here we consider InAsSb, a highly doped semiconductor whose plasma frequency can be tuned by playing with the doping concentration. In that case, the plasma frequency is in the infrared. The hyperbolic behavior of the multilayer can thus be expected to occur only below the plasma frequency. This material is in addition compatible with CMOS technology and its relative permittivity is given by a $\epsilon_m = \epsilon_\infty\{1 - \omega_p^2/[\omega(\omega + i\gamma)]\}$ with $\epsilon_\infty = 11.7$, $\omega_p = 351 \times 10^{12}$ rad s$^{-1}$ and $\gamma = 10^{13}$ rad s$^{-1}$ [39–41]. The dielectric between the InAsSb layers is GaSb, a dielectric whose permittivity $\epsilon_d = 13.4$ can be considered constant [42].

For $p$-polarized light (the magnetic field being perpendicular to the $x$-$z$ plane) and in the long-wavelength limit ($\lambda \gg D$) the multilayer behaves as a homogeneous anisotropic medium, characterized by a permittivity tensor whose relative principal elements are given by

$$\epsilon_\perp = (1-\rho)\epsilon_m + \rho\epsilon_d, \qquad \epsilon_z = \left(\frac{1-\rho}{\epsilon_m} + \frac{\rho}{\epsilon_d}\right)^{-1} \tag{1}$$

with $\epsilon_x = \epsilon_y = \epsilon_\perp$. Within the HM, electromagnetic waves thus satisfy the dispersion relation:

$$k_x^2/\epsilon_z + k_y^2/\epsilon_z + k_z^2/\epsilon_x = k_0^2, \tag{2}$$

where $k_0$ is the wave number in vacuum. To understand the optical properties of HWs, we first analyze the guided modes propagating in a one-dimensional waveguide made of two metallic planes filled by a HM of type-II ($\epsilon_z > 0$ and $\epsilon_\perp < 0$). The structure presented in the inset of Fig. 3(b) is invariant in the $y$ and $x$ directions, while perfect boundary conditions are assumed for $z = 0$ and $z = g$. Looking for guided modes propagating in the ordinary $x$ direction, a straightforward calculus leads us to conclude that several modes can be supported by the waveguide, characterized by an integer $m$, the order of the mode. The magnetic field associated with the $m$th guided mode (for $p$ polarization) can be written

$$H_y^{(m)} = H_0 \cos\left(m\frac{\pi}{g}z\right)e^{-ik_x^{(m)}x}, \tag{3}$$

where $k_x^{(m)}$ is the propagation constant along the $x$ direction and $H_0$ its (arbitrary) amplitude. Using Eq. (2), the effective

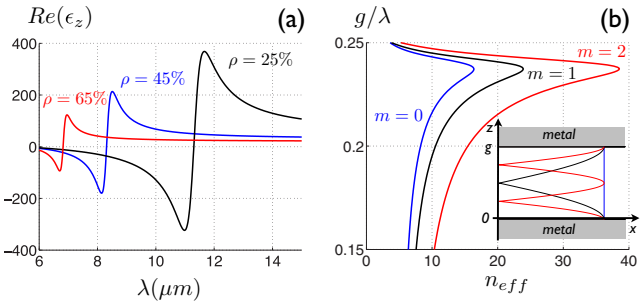


FIG. 3. (a) Real part of $\epsilon_z$ as a function of the wavelength and for three compositions $\rho$ of 25%, 45%, and 65%. (b) Dispersion relation of the three first modes ($m = 0,1,2$) as a function of the reduced frequency $g/\lambda$. The inset represents the modulus of the magnetic field [Eq. (3)] associated with the three lowest-order modes in a $g = 2$ $\mu$m wide waveguide. Blue, black, and red modes correspond, respectively, to $m = 0,1,2$.

index of the $m$th mode defined by $n_{\text{eff}}^{(m)} = k_x^{(m)}/k_0$ is then given by

$$n_{\text{eff}}^{(m)} = \sqrt{\epsilon_z}\sqrt{1 - \frac{1}{\epsilon_\perp}\left(\frac{m\lambda}{2g}\right)^2}. \tag{4}$$

This result shows that the effective index of a guided mode is mostly driven by the value taken by the extraordinary permittivity $\epsilon_z$. This quantity is shown on Fig. 3(a) as a function of the wavelength for different values of $\rho$, the dielectric filling ratio. The real part of $\epsilon_z$ presents a maximum that redshifts and reaches very high values when the filling ratio decreases, offering to control and to tune this crucial parameter. Figure 3(b) shows the effective indices given by Eq. (4) reached by the three lowest-order guided modes propagating inside a $g = 2$ $\mu$m wide waveguide. For the lossless metallic case, these high-$k$ guided modes, which can be connected to bulk hyperbolic plasmons [31,38], present a maximal effective index at the effective frequency $\omega_{\text{eff}}$ obtained when $\epsilon_z \to +\infty$:

$$\omega_{\text{eff}} = \omega_p\left(1 + \frac{(1-\rho)}{\rho}\frac{\epsilon_d}{\epsilon_\infty}\right)^{-1/2}. \tag{5}$$

This result is in agreement with the redshift observed for the maximal $\text{Re}(\epsilon_z)$ at the effective wavelength $2\pi c/\omega_{\text{eff}}$ when $\rho$ decreases [Fig. 3(a)]. Since the resonant frequency of HWs arises in the slow light regime, i.e., close to the effective frequency, we are able to derive the theoretical size reduction of a resonator sustaining the $m$th resonance: $m_p^{(m)} = 2\text{Re}[n_{\text{eff}}^{(m)}(\omega_{\text{eff}})]$. The miniaturization parameter for that HW supporting the fundamental TEM mode (which resembles the fundamental BPP mode [25]) is hence given by

$$m_p^{(0)} = 2\text{Re}(\sqrt{\epsilon_z(\omega_{\text{eff}})}). \tag{6}$$

By decreasing the amount of dielectric material in the composition of the HW, the resonance is shifted over a broad range of frequency, while the wire is drastically miniaturized, as shown Fig. 4. For a very small filling fraction of dielectric about 1%, it is predicted that the fundamental resonant wavelength is more than 100 times larger than the width of the HW, thus exceeding the usual limit imposed to MIM resonators [Fig. 4(b)].

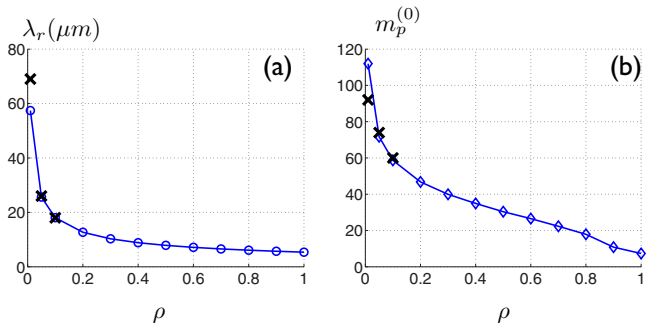


FIG. 4. (a) Theoretical resonant wavelength of the HW for the fundamental mode as a function of the filling ratio in dielectric $\rho$. (b) Miniaturization factor given by Eq. (6) for a HW resonating with the fundamental mode as a function of $\rho$. Black crosses correspond to the results obtained for the 3D simulations.

This simple physical picture is validated by comparing the response of composite HW to the response of a patch antenna in which the multilayer is replaced by a spacer made of an equivalent homogeneous hyperbolic medium (Fig. 5). Here, we still consider the 2D case depicted in Fig. 2(a) where the antennas are periodically settled in the $x$ direction with a pitch $d = 1$ $\mu$m. For a filling factor $\rho = 45\%$, the theoretical fundamental resonant wavelength is found around $\lambda_r^{(0)} = 8.5$ $\mu$m where $\text{Re}(\epsilon_z)$ attains its maximal value of 213 [Fig. 3(a)]. According to Eq. (6), the width of the metallic patch is chosen to be $w = 300$ nm for a thickness $t = 350$ nm. The height of the HW is $g = 2$ $\mu$m and it is made of 40 metallic and dielectric films of respective thicknesses $h_m = 27.5$ nm and $h_d = 22.5$ nm. The absorption spectra are calculated with a finite element method solver (COMSOL MULTIPHYSICS) when the structure is illuminated by a plane wave in normal incidence with a magnetic field oriented in the invariant $y$ direction ($p$ polarization) [Fig. 5(a)]. Good agreement is observed for the absorption spectra as well as for the magnetic field maps [Fig. 5(b)]. It appears three resonances associated to the fundamental mode $\text{TM}_0$ (at $\lambda = 8.7$ $\mu$m), the first odd mode $\text{TM}_1$ (at $\lambda = 9.5$ $\mu$m), and the second even mode $\text{TM}_2$ (at $\lambda = 11.2$ $\mu$m). The spatial extensions of these resonant modes

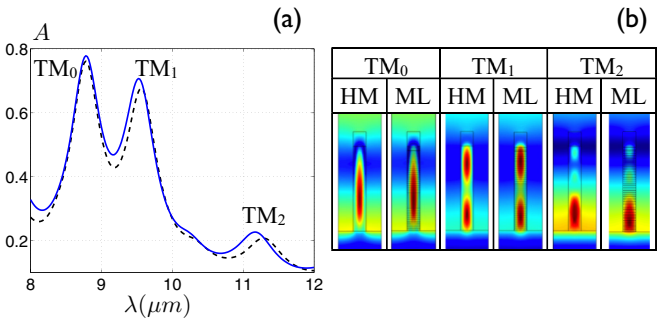


FIG. 5. (a) Absorption spectrum calculated for a metal-dielectric multilayer spacer (solid curve) and for a homogeneous HM spacer (dashed curve). (b) Modulus of the magnetic field calculated for the three first resonant modes. The columns labeled HM and ML correspond, respectively, to a homogeneous HM spacer and a multilayer one.

agree with bulk plasmon polariton (BBP) modes obtained for the HM waveguide depicted in the inset of Fig. 3(b). We also notice that the calculated resonant wavelength for the fundamental mode is close to the theoretical one $\lambda_r^{(0)} = 8.5\ \mu$m.

These results obtained when the HWs are ended by a metallic patch whose thickness $t = 350$ nm exceeds the penetration distance for the waves into the metal (about 200 nm) demonstrate that the resonances at work inside HWs are based on stationary BPP modes resonating in the ordinary $x$ direction. However, similar properties are obtained when the metallic patch is removed. Its presence is nevertheless convenient because it allows one to analyze the HW in terms of guided modes having effective indices given by Eq. (4). We also notice that if BPP modes can be coupled to radiative waves by a grating deposited above a uniform HM layer as for hypergrating structures [35], the miniaturization effect observed for a HW originates from the formation of stationary BPP waves confined in a cavity whose width is determined by Eq. (6). More generally, a stronger miniaturization effect is seen for HWs than for isotropic metallic wires. The latter support localized surface-plasmon resonances along or at their top end according to the geometry [43,44]. For similar structures consisting of a periodic set of metallic nanorods standing on a metallic plate, the electric field enhancement is associated to an absorption efficiency of 90% for a miniaturization factor of about 25 which is four times smaller than that for HWs [45]. Even if the control of the spectral properties of nanowires is envisaged by adjusting the doping level of semiconductors [46,47], HMs offer an original alternative to synthesize at demand highly miniaturized nanowires made of predetermined dielectric and metallic materials.

## III. 3D SIMULATIONS OF HYPERBOLIC WIRES

We now extend the previous results to the case of 3D HWs periodically arranged in a square lattice in the $x$-$y$ plane with a pitch $d$ in both directions. We focus, in particular, on small dielectric filling factors in order to conceive highly miniaturized HWs. The period of the multilayer is chosen to be $D = 100$ nm while $\rho$ is decreased from 10%, 5%, to 1%. For each case the thickness $g$, the period $d$, and the width $w$ of the wires are optimized to get an absorption efficiency higher than 90% attributed to the resonance of the fundamental BPP mode. We remark that the thickness of the metallic patch is kept constant to 350 nm in these 3D electromagnetic simulations realized with a homemade code based on the rigorous coupled-wave analysis method [48]. The absorption spectra calculated in normal incidence show a shift for the fundamental resonance wavelength from 18 to 69 $\mu$m when the filling factors are varied for $\rho = 10\%$ to $\rho = 1\%$ [Fig. 6(a)]. The geometrical parameters and miniaturization parameter obtained for these different filling ratios are summarized in Table I. Highly miniaturized HWs presenting a large aspect ratio $g/w$ might be challenging from the fabrication point of view. However, complex structures such as thick photonic crystals reaching aspect ratios about 4 have already been fabricated with a time-multiplexed etching process

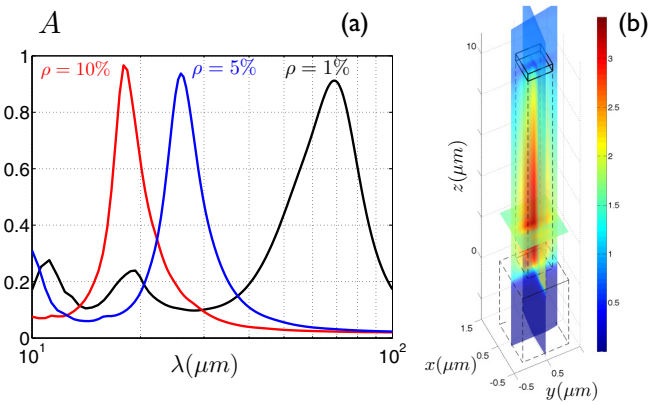


FIG. 6. (a) Absorption spectra in a logarithm scale calculated for three hyperbolic wires of filling ratio in dielectric $\rho = \{1\%,5\%,10\%\}$ (respectively, the black, blue, and red curves). (b) Modulus of the magnetic field for $\rho = 1\%$ at the resonant wavelength $\lambda = 69\ \mu$m.

[49,50]. Moreover, the current molecular beam epitaxy process allows the deposition of multilayers whose thicknesses are controlled at the monoatomic resolution, i.e., for a 0.3 nm typical error. Since HWs work in the homogenization regime, their optical properties are robust against these small fluctuations even in the extreme miniaturization regime.

In this latter case, for $\rho = 1\%$, the 3D map of the magnetic field modulus plotted in Fig. 6(b) at $\lambda_r = 69\ \mu$m proves that the resonant absorption can actually be attributed to the fundamental BPP mode. The resonant wavelength and the miniaturization parameter obtained for these 3D simulations are compared in Fig. 4 to the theoretical calculations obtained with the effective model developed in Sec. II. The good agreement between these results demonstrates that our simple picture is still valid for 3D structures, and that the resonant wavelength can be shifted over a broad range of wavelength by controlling the composition in dielectric of the hyperbolic metamaterial. We underline that the width of the HW is reduced to only one hundredth of the resonance wavelength (one order of magnitude smaller than for a MIM resonator), while preserving a large efficiency. The absorption is actually almost perfect whatever the resonance wavelength, which is very different from what occurs for regular MIM structures. Let us finally remark that similarly to MIM antennas, the fluctuation of the HW width should result in a broadening of the absorption line [17].

TABLE I. Geometrical parameters, resonant wavelengths, and miniaturization parameter for 3D hyperbolic wires presenting three metal-dielectric composition $\rho$.

| $\rho$ | $d$ ($\mu$m) | $g$ ($\mu$m) | $w$ (nm) | $\lambda_r$ ($\mu$m) | $m_p^{(0)}$ |
|---|---|---|---|---|---|
| 10% | 0.4 | 2 | 300 | 17 | 60 |
| 5% | 0.5 | 3.5 | 350 | 26 | 74 |
| 1% | 1.4 | 10 | 750 | 69 | 92 |

## IV. CONCLUSION

We have thoroughly studied the electromagnetic response of hyperbolic wires made of a highly doped semiconductor and a dielectric material. We have provided a simple yet very accurate physical picture of their behavior, showing that BPP modes having very high effective indices can be squeezed inside deeply subwavelength resonators. This leads to an extreme miniaturization of HWs to only one hundredth of the wavelength while maintaining a very high absorption efficiency. The modification in their dielectric and metallic fractions provides a versatile way to shift the absorption line over a wide range of wavelength [10–100] $\mu$m. Thanks to this physical analysis, we are confident that HWs can be used in other frequency ranges and with other materials (such as noble metals). Since the design we propose allows one to overcome the major limitations of standard plasmonic resonators such as MIM or nanowire antennas, we hope hyperbolic wires will be useful for numerous applications.

## ACKNOWLEDGMENTS

This work is supported by the Agence Nationale de la Recherche of France, project Physics of Gap-Plasmons (ANR-13-JS10-0003). The authors would like to thank Kofi Edee for its support for the 3D electromagnetic simulations.

[1] P. Bharadwaj, B. Deutsch, and L. Novotny, Adv. Opt. Photon. **1**, 438 (2009).
[2] A. Shaltout, J. Liu, A. Kildishev, and V. Shalaev, Optica **2**, 860 (2015).
[3] K. C. Y. Huang, M.-K. Seo, T. Sarmiento, Y. Huo, J. S. Harris, and M. L. Brongersma, Nat. Photon. **8**, 244 (2014).
[4] A. Pors, O. Albrektsen, I. P. Radko, and S. I. Bozhevolnyi, Sci. Rep. **3**, 2155 (2013).
[5] A. Cattoni, P. Ghenuche, A.-M. Haghiri-Gosnet, D. Decanini, J. Chen, J.-L. Pelouard, and S. Collin, Nano Lett. **11**, 3557 (2011).
[6] N. Vandamme, H.-L. Chen, A. Gaucher, B. Behaghel, A. Lemaître, A. Cattoni, C. Dupuis, N. Bardou, J.-F. Guillemoles, and S. Collin, IEEE J. Photovolt. **5**, 565 (2015).
[7] R. Esteban, T. V. Teperik, and J. J. Greffet, Phys. Rev. Lett. **104**, 026802 (2010).
[8] S. I. Bozhevolnyi and T. Sndergaard, Opt. Express **15**, 10869 (2007).
[9] J. Yang, C. Sauvan, A. Jouanin, S. Collin, J.-L. Pelouard, and P. Lalanne, Opt. Express **20**, 16880 (2012).
[10] R. Smaali, F. Omeis, A. Moreau, T. Taliercio, and E. Centeno, Sci. Rep. **6**, 32589 (2016).
[11] M. Miyata, A. Holsteen, Y. Nagasaki, M. L. Brongersma, and J. Takahara, Nano Lett. **15**, 5609 (2015).
[12] C. Tserkezis, R. Esteban, D. O. Sigle, J. Mertens, L. O. Herrmann, J. J. Baumberg, and J. Aizpurua, Phys. Rev. A **92**, 053811 (2015).
[13] S. Collin, F. Pardo, and J.-L. Pelouard, Opt. Express **15**, 4310 (2007).
[14] I. Puscasu and W. L. Schaich, Appl. Phys. Lett. **92**, 233102 (2008).
[15] F. Pardo, P. Bouchon, R. Haidar, and J.-L. Pelouard, Phys. Rev. Lett. **107**, 093902 (2011).
[16] G. M. Akselrod, J. Huang, T. B. Hoang, P. T. Bowen, L. Su, D. R. Smith, and M. H. Mikkelsen, Adv. Mater. **27**, 8028 (2015).
[17] A. Moreau, C. Ciraci, J. J. Mock, R. T. Hill, Q. Wang, and B. J. Wiley, Nature (London) **492**, 86 (2012).
[18] R. Chikkaraddy, B. de Nijs, F. Benz, S. J. Barrow, O. A. Scherman, E. Rosta, A. Demetriadou, P. Fox, O. Hess, and J. J. Baumberg, Nature (London) **535**, 127 (2016).
[19] F. Bigourdan, F. Marquier, J. P. Hugonin, and J. J. Greffet, Opt. Express **22**, 2337 (2014).
[20] A. Lefebvre, D. Costantini, I. Doyen, Q. Lévesque, E. Lorent, D. Jacolin, J. J. Greffet, S. Boutami, and H. Benisty, Opt. Mater. Express **6**, 2389 (2016).
[21] T. B. Hoang, G. M. Akselrod, C. Argyropoulos, J. Huang, D. R. Smith, and M. H. Mikkelsen, Nat. Commun. **6**, 7788 (2015).
[22] G. M. Akselrod, C. Argyropoulos, T. B. Hoang, C. Ciraci, C. Fang, J. Huang, D. R. Smith, and M. H. Mikkelsen, Nat. Photon. **8**, 835 (2014).
[23] C. Guclu, T. S. Luk, G. T. Wang, and F. Capolino, Appl. Phys. Lett. **105**, 123101 (2014).
[24] R. Alaee, C. Menzel, U. Huebner, E. Pshenay-Severin, S. Bin Hasan, T. Pertsch, C. Rockstuhl, and F. Lederer, Nano Lett. **13**, 3482 (2013).
[25] I. Avrutsky, I. Salakhutdinov, J. Elser, and V. Podolskiy, Phys. Rev. B **75**, 241402 (2007).
[26] D. R. Smith and D. Schurig, Phys. Rev. Lett. **90**, 077405 (2003).
[27] L. Ferrari, C. Wu, D. Lepage, X. Zhang, and Z. Liu, Prog. Quantum Electron. **40**, 1 (2015).
[28] Y. Guo, W. Newman, C. L. Cortes, and Z. Jacob, Adv. OptoElectron. **2012**, 9 (2012).
[29] V. Caligiuri, R. Dhama, K. V. Sreekanth, G. Strangi, and A. De Luca, Sci. Rep. **6**, 20002 (2016).
[30] A. A. High, R. C. Devlin, A. Dibos, M. Polking, D. S. Wild, J. Perczel, N. P. de Leon, M. D. Lukin, and H. Park, Nature (London) **522**, 192 (2015).
[31] N. Vasilantonakis, M. E. Nasir, W. Dickson, G. A. Wurtz, and A. V. Zayats, Laser Photon. Rev. **9**, 345 (2015).
[32] R. Maas, J. van de Groep, and A. Polman, Optica **3**, 592 (2016).
[33] E. Centeno and A. Moreau, Phys. Rev. B **92**, 045404 (2015).
[34] C. Long, S. Yin, W. Wang, W. Li, J. Zhu, and J. Guan, Sci. Rep. **6**, 21431 (2016).
[35] K. V. Sreekanth, A. De Luca, and G. Strangi, Sci. Rep. **3**, 3291 (2013).
[36] H. Zhu, X. Yin, L. Chen, Z. Zhu, and X. Li, Opt. Lett. **40**, 4595 (2015).
[37] H. Hu, D. Ji, X. Zeng, K. Liu, and Q. Gan, Sci. Rep. **3**, 1249 (2013).
[38] S. V. Zhukovsky, O. Kidwai, and J. E. Sipe, Opt. Express **21**, 14982 (2013).
[39] V. N'Tsame Guilengui, L. Cerutti, J. B. Rodriguez, E. Tournié, and T. Taliercio, Appl. Phys. Lett. **101**, 161113 (2012).

[40] T. Taliercio, V. N. Guilengui, L. Cerutti, E. Tournié, and J-J. Greffet, Opt. Express **22**, 24294 (2014).
[41] M. J. Milla, F. Barho, F. González-Posada, L. Cerutti, M. Bomers, J. B. Rodriguez, E. Tournié, and T. Taliercio, Nanotechnology **27**, 425201 (2016).
[42] S. Roux, P. Barritault, O. Lartigue, L. Cerutti, E. Tournié, B. Gérard, and A. Grisard, Appl. Phys. Lett. **107**, 171901 (2015).
[43] J. Dorfmüller, R. Vogelgesang, W. Khunsin, C. Rockstuhl, C. Etrich, and K. Kern, Nano Lett. **10**, 3596 (2010).
[44] T. Kang, W. Choi, I. Yoon, H. Lee, M.-K. Seo, Q.-H. Park, and B. Kim, Nano Lett. **12**, 2331 (2012).
[45] M. Malerba, A. Alabastri, E. Miele, P. Zilio, M. Patrini, D. Bajoni, G. C. Messina, M. Dipalo, T. Sarmiento, R. P. Zaccaria, and F. De Angelis, Sci. Rep. **5**, 16436 (2015).
[46] L.-W. Chou, N. Shin, S. V. Sivaram, and M. A. Filler, J. Am. Chem. Soc. **134**, 16155 (2012).
[47] D. S. Boyuk, L.-W. Chou, and M. A. Filler, ACS Photon. **3**, 184 (2016).
[48] T. Weiss, G. Granet, N. A. Gippius, and S. G. Tikhodeev, Opt. Express **17**, 8051 (2009).
[49] S. Moumdji, A. Larrue, D. Belharet, P. Dubreuil, S. Bonnefont, O. Gauthier-Lafaye, Y. Rouillard, and A. Vicet, Electron. Lett. **45**, 1119 (2009).
[50] M. Jahjah, S. Moumdji, O. Gauthier-Lafaye, S. Bonnefont, Y. Rouillard, and A. Vicet, Electron. Lett. **48**, 277 (2012).